Influence of capillary pressure on CO_2 storage and monitoring

Juan E. Santos, CONICET, Instituto del Gas y del Petróleo, Facultad Ingeniería, Universidad de Buenos Aires, Department of Mathematics, Purdue University and Universidad Nacional de La Plata, Argentina, Gabriela B. Savioli, Lucas A. Macías, Instituto del Gas y del Petróleo, Facultad Ingeniería, Universidad de Buenos Aires, José M. Carcione and Davide Gei, Istituto Nazionale di Oceanografia e di Geofisica Sperimentale - OGS, Italy*

SUMMARY

Sequestration of CO_2 in geological formations is one of the solutions to mitigate the greenhouse effect. We are interested in analyzing the influence of capillary pressure on CO_2 injection, storage and monitoring in saline aquifers. To do so, we present a methodology integrating numerical simulation of CO_2- brine flow and seismic wave propagation. Besides, we build a suitable geological model that includes mudstone layers and fractures. The simultaneous flow of CO_2 and brine in porous media is described by the Black-Oil formulation, which applies a simplified thermodynamic model. Capillary pressure is represented as a potential function of CO_2 saturation. The wave propagation is simulated using a viscoelastic model that includes attenuation and dispersion effects due to mesoscopic scale heterogeneities. The fluid simulator properly models the CO_2 injection, obtaining accumulations below the mudstone layers as injection proceeds. We are able to identify the time-lapse distribution of CO_2 from the synthetic seismograms, which show the typical pushdown effect. When capillary pressure is higher, CO_2 upward migration is slower and thicker zones of CO_2 accumulations are obtained. Numerical examples show the effectiveness of this methodology to detect the spatio-temporal distribution of CO_2 and to make long term predictions.

INTRODUCTION

Capture and storage of CO_2 in deep saline aquifers is a valid alternative for reducing the amount of greenhouse gases in the atmosphere (Arts et al., 2008). The first industrial CO_2 injection project is the Sleipner gas field, where CO_2 separated from natural gas is being injected in the Utsira formation, a highly permeable porous sandstone (Arts et al., 2008)-(Chadwick et al., 2005) with several mudstone layers which act as barriers to the vertical flow of the CO_2. Numerical modeling of CO_2 injection and seismic monitoring are important tools to understand the long term behavior after injection and to test the effectiveness of CO_2 sequestration. Recent papers (Carcione and Picotti, 2006)-(Carcione et al., 2012) successfully apply seismic modeling for monitoring the spatio-temporal distribution of CO_2 using assumed saturation maps. Instead, we introduce a methodology to model the gas flow and monitor the storage.We also build a petrophysical model of the Utsira formation based on fractal porosity and clay content, taking into account the variation of properties with pore pressure and saturation (Carcione et al., 2003). The simultaneous flow of brine and CO_2 is modeled with the Black-Oil formulation for two-phase flow in porous media (Aziz and Settari, 1985), which uses the PVT data as a simplified thermodynamic model (Hassanzadeh et al., 2008). The wave propagation is based on an isotropic viscoelastic model that considers dispersion and attenuation effects. The complex P-wave and S-wave moduli are determined using the Zener model in the brine saturated mudstone layers (Carcione, 2007); and the White's theory (White et al., 1975) in zones saturated with brine and CO_2. The results of the flow simulator, allows us to calculate the phase velocities and attenuation coefficients of the P and S waves in order to compute the synthetic seismograms. The methodology is used to model CO_2 injection and flow and compute time-lapse seismograms corresponding to the Utsira aquifer at Sleipner field applying different capillary pressure curves.

CO_2 - BRINE FLOW MODEL IN POROUS MEDIA

The well-known Black-Oil formulation applied to two-phase, two component fluid flow (Aziz and Settari, 1985) is used to simulate the simultaneous flow of brine (subindex b) and CO_2 (subindex g), considering that CO_2 may dissolve in the brine but the brine is not allowed to vaporize into the CO_2 phase. This formulation uses the PVT data (R_s: CO_2 solubility in brine; B_g and B_b: CO_2 and brine formation volume factors) as a simplified thermodynamic model, computed with the Hassanzadeh correlations (Hassanzadeh et al., 2008). Combining the mass conservation equations with Darcy's empirical Law, the following nonlinear system of partial differential equations is obtained,

$$\nabla\cdot(\underline{\kappa}(\frac{\kappa_{rg}}{B_g\eta_g}(\nabla p_g-\rho_g g\nabla D)+\frac{R_s\kappa_{rb}}{B_b\eta_b}(\nabla p_b-\rho_b g\nabla D)))+\frac{q_g}{\rho_g^{SC}}=\frac{\partial\left[\phi\left(\frac{S_g}{B_g}+\frac{R_sS_b}{B_b}\right)\right]}{\partial t}, \quad (1)$$

$$\nabla\cdot(\underline{\kappa}\frac{\kappa_{rb}}{B_b\eta_b}(\nabla p_b-\rho_b g\nabla D))+\frac{q_b}{\rho_b^{SC}}=\frac{\partial\left[\phi\frac{S_b}{B_b}\right]}{\partial t}. \quad (2)$$

Here $\underline{\kappa}$ is the absolute permeability tensor, p_g, p_b are the fluid pressures and for $\beta=g,b$, $k_{r\beta}$ and η_β are the relative permeability and viscosity of the β-phase, respectively. Two algebraic equations relating the saturations and pressures, complete the system:

$$S_b+S_g=1, \qquad p_g-p_b=PC(S_b), \quad (3)$$

where PC is the capillary pressure. The relationship between capillary pressure and CO_2 saturation may be represented by the following potential function:

$$PC(S_g)=PC_{max}(\frac{S_g-S_{gc}}{1-S_{gc}-S_{bc}})^{n_c}, \quad (4)$$

where S_{gc} and S_{bc} are the saturations at which CO_2 and brine phases become mobile, respectively.

The solution of the Black-Oil model is obtained employing the public domain software BOAST (Fanchi, 1997) which solves the differential equations using the IMPES algorithm (IMplicit Pressure Explicit Saturation), based on a finite difference technique (Aziz and Settari, 1985).

SEISMIC MODELING

Mesoscopic attenuation effects

An important mechanism of P-wave attenuation and dispersion at seismic frequencies is known as mesoscopic loss, due to heterogeneities larger than the pore size but much smaller than the predominant wavelengths (mesoscopic-scale heterogeneities). Due to the extremely fine meshes needed to properly represent these type of media, numerical simulation at the macroscale is very expensive or even not feasible. Our approach to solve this problem consists in applying an upscaling procedure to include the mesoscale effects in the macroscale (Santos et al., 2008). Within the formation, in zones where CO_2 is present, we determine complex and frequency dependent P-wave modulus $E(\omega) = \lambda(\omega) + 2\mu(\omega)$ at the mesoscale using White's theory for patchy saturation (White et al., 1975), where $\lambda(\omega)$ and $\mu(\omega)$ are the Lamé coefficients and ω is the angular frequency. Shear wave attenuation is taken into account using another relaxation mechanism, related to the P-wave White mechanism, to make the shear modulus $\mu(\omega)$ complex and frequency dependent. Outside the formation and in zones where only brine is present, the complex bulk and shear moduli as function of frequency are determined using a Zener model. These complex moduli define an equivalent viscoelastic model at the macroscale that takes into account dispersion and attenuation effects occurring at the mesoscale.

Constitutive Relations

Let $u = u(\omega) = (u_x(\omega), u_z(\omega))$ be the time-Fourier transform of the displacement vector. Therefore, the stress-strain relations in the space-frequency domain are:

$$\sigma_{jk}(u) = \lambda(\omega)\nabla\cdot u\,\delta_{jk} + 2\mu(\omega)\varepsilon_{jk}(u), \qquad (5)$$

where $\sigma_{jk}(u)$ is the stress tensor, $\varepsilon_{jk}(u)$ is the strain tensor, δ_{jk} is the Kroenecker delta, and $\lambda(\omega), \mu(\omega)$ are the complex Lamé coefficients determined using White's theory.

Phase velocities and attenuation coefficients

For isotropic viscoelastic solids, the frequency dependent phase velocities $v_t(\omega)$ and quality factors $Q_t(\omega)$ ($t = p, s$) are defined by the relations

$$v_t(\omega) = \left[\mathrm{Re}\left(\frac{1}{vc_t(\omega)}\right)\right]^{-1}, Q_t(\omega) = \frac{\mathrm{Re}(vc_t(\omega)^2)}{\mathrm{Im}(vc_t(\omega)^2)}, \qquad (6)$$

where $vc_p(\omega), vc_s(\omega)$ are the complex and frequency dependent compressional and shear velocities defined as

$$vc_p(\omega) = \sqrt{\frac{E(\omega)}{\rho}}, \quad vc_s(\omega) = \sqrt{\frac{\mu(\omega)}{\rho}} \qquad (7)$$

with ρ the bulk density.

A viscoelastic model for wave propagation

The equation of motion in a 2D isotropic viscoelastic domain Ω with boundary $\partial\Omega$ is (Santos et al., 2008) :

$$\omega^2\rho u + \nabla\cdot\sigma(u) = f(x,\omega), \quad \Omega, \qquad (8)$$

with first-order absorbing boundary condition:

$$-\sigma(u)\nu = i\omega\mathscr{D}u, \quad \partial\Omega. \qquad (9)$$

Here $f(x,\omega)$ is the external source and $\mathscr{D}$ is a positive definite matrix which definition is given in (Ha et al., 2002).

The numerical solution is computed at a selected number of frequencies in the range of interest using an iterative finite element domain decomposition procedure. The time domain solution is obtained using a discrete inverse Fourier transform (Ha et al., 2002) . To approximate each component of the solid displacement vector we employ a nonconforming finite element space which generates less numerical dispersion than the standard bilinear elements.

PETROPHYSICAL MODEL OF A SHALY SANDSTONE

The pressure dependence of properties is based on the following relationship between porosity and pore pressure $p(t) = S_b p_b(t) + S_g p_g(t)$,

$$\frac{(1-\phi_c)}{K_s}(p(t) - p_H) = \phi_0 - \phi(t) + \phi_c \ln\frac{\phi(t)}{\phi_0}, \qquad (10)$$

where ϕ_c is a critical porosity, ϕ_0 is the initial porosity at hydrostatic pore pressure p_H and K_s is the bulk modulus of the solid grains (Carcione et al., 2003). The rock is formed with quartz (bulk modulus of 40 GPa) and clay (bulk modulus of 15 GPa). K_s is computed as the arithmetic average of the Hashin Shtrikman upper and lower bounds. The relationship among horizontal permeability, porosity and clay content C is (Carcione et al., 2003) ,

$$\frac{1}{\kappa_x(t)} = \frac{45(1-\phi(t))^2}{\phi(t)^3}\left(\frac{(1-C)^2}{R_q^2} + \frac{C^2}{R_c^2}\right), \qquad (11)$$

where R_q and R_c are the average radii of the sand and clay grains. Also, as permeability is anisotropic, we assume the following relationship between horizontal and vertical permeability κ_z (Carcione et al., 2003)

$$\frac{\kappa_x(t)}{\kappa_z(t)} = \frac{1-(1-0.3a)\sin\pi S_b}{a(1-0.5\sin\pi S_b)}, \qquad (12)$$

where a is the permeability-anisotropy parameter. The bulk modulus of the dry matrix, K_m, is computed using the Krief equation (Krief et al., 1990) as follows:

$$K_m(t) = K_s(1-\phi(t))^{A/(1-\phi(t))}. \qquad (13)$$

Assuming a relation $K_m/\mu_m = K_s/\mu_s$, we set

$$\mu_m(t) = \mu_s(1-\phi(t))^{A/(1-\phi(t))}. \qquad (14)$$

Using the moduli K_s, K_m, μ_m, the porosity ϕ and permeabilities κ_x, κ_z, as well as the fluids bulk moduli and viscosities (computed using the Peng-Robinson model (Peng and Robinson, 1976)), we determine the complex and frequency dependent Lamé coefficients $\lambda(\omega), \mu(\omega)$ as explained before.

EXAMPLES

To test the proposed methodology, we consider a model of the Utsira formation having 1.2 km in the *x*-direction, 10 km in the *y*-direction and 0.4 km in the *z*-direction (top at 0.77 km and bottom at 1.17 km b.s.l.). The pressure-temperature conditions are $T = 31.7z + 3.4$, where T is the temperature (in ^oC) and z is the depth (in km b.s.l.); $p_H = \rho_b g z$ is the hydrostatic pressure, with ρ_b = 1040 kg/m^3 the density of brine and g the gravity constant. Within the formation, there are several mudstone layers which act as barriers to the vertical motion of the CO_2. The initial porosity ϕ_0 (at hydrostatic pore pressure) for the Utsira sandstone is assumed to have a fractal spatial distribution, based on the so-called von Karman self-similar correlation functions (Frankel and Clayton, 1986). Horizontal and vertical permeabilities were determined by using equations (11) and (12), considering an anisotropy parameter a = 0.1 and a fixed clay content C = 6 %. We describe the results obtained using two different capillary pressure curves, that are shown in Figure 1.

- PC_{max}=30 kPa, n_c=4
- PC_{max}=100 kPa, n_c=2

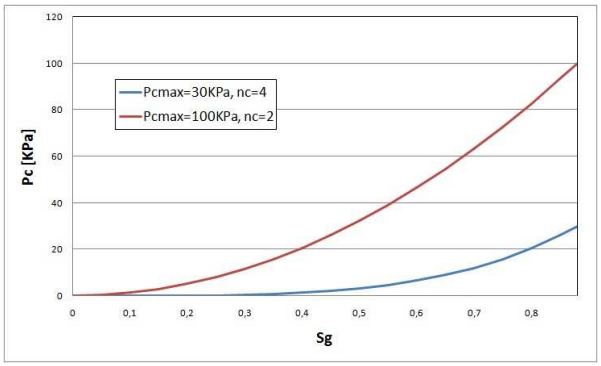

Figure 1: Capillary pressure curves.

CO_2 injection

CO_2 is injected during seven years in the Utsira formation at a constant flow rate of one million tons per year. The injection point is located at the bottom of the formation: x = 0.6 km, z =1.082 km. The simulation uses a mesh with equally-spaced blocks in each direction: $n_x = 300$ in the *x*-direction, $n_y = 5$ in the *y*-direction and $n_z = 400$ in the *z*-direction. Actually the model is 2.5D since the properties are uniform along the *y*-direction, which has an extension of 10 km. The source is located at the third grid point along this direction. To satisfy the CFL stability condition due to IMPES formulation (Savioli and Bidner, 2005), the time step is 0.05 d. Recall that the petrophysical properties of the formation are time dependent due to the CO_2 injection and consequent increase in pore fluid pressure, but they change at a much slower rate than pressure and saturations. As a consequence, we have two time scales, and we use a much larger time step to update petrophysical properties than to run the flow simulator. In this work, the petrophysical properties are updated every year.

Figures 2(a) and 3(a) show 2D vertical slices (corresponding to $n_y = 3$) of the CO_2 saturation fields after three years of CO_2 injection, computed using the lower and higher *PC* curves, respectively. In both cases, CO_2 accumulations below the mudstone layers can be observed. As injection proceeds, part of the injected fluid migrates upwards due to the openings in the mudstone layers that generate chimneys. Comparing both figures, when capillary pressure is higher, CO_2 upward migration is slower and, consequently, we can observe thicker zones of accumulations below the layers and high CO_2 saturations levels between layers.

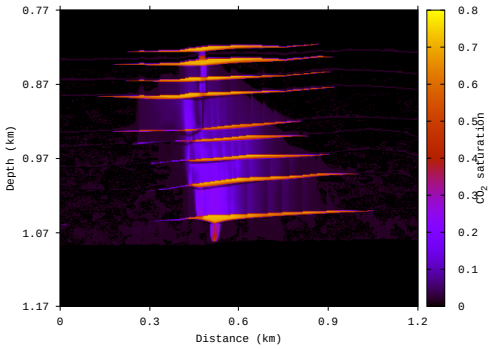

(a)

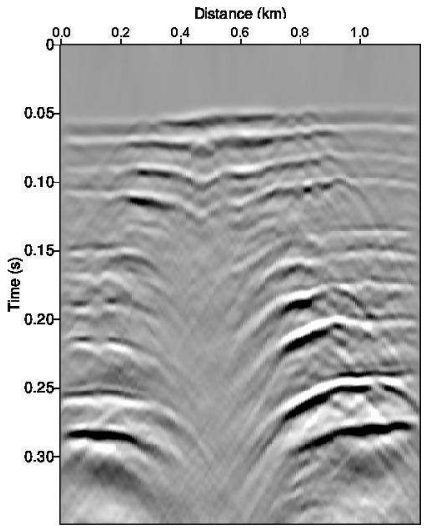

(b)

Figure 2: CO_2 saturation distribution and synthetic seismogram after three years of CO2 injection. Lower capillary pressure, PC_{max}=30 kPa, n_c=4.

Seismic Monitoring

In this section, we analyze the capability of seismic monitoring to identify zones of CO_2 accumulation and migration. With this purpose, we use 2D slices of CO_2 saturation and fluid pressure obtained from the flow simulator to construct a 2D model of the Utsira formation. The seismic source is a spatially lo-

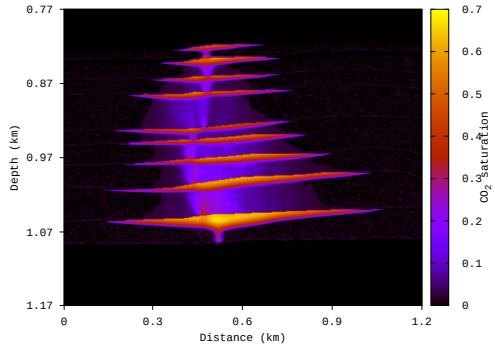

(a)

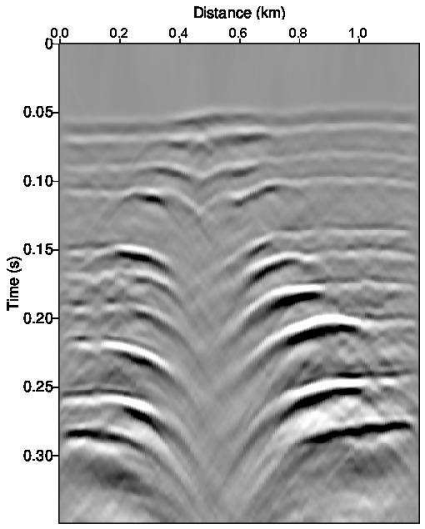

(b)

Figure 3: CO_2 saturation distribution and synthetic seismogram after three years of CO2 injection. Higher capillary pressure, PC_{max}=100 kPa, n_c=2.

calized plane wave of main frequency 60 Hz. Figures 2(b) and 3(b) display seismograms after three of CO_2 injection associated with the CO_2 saturations shown in Figures 2(a) and 3(a), respectively. A standard f-k filter is applied to the seismic sections. The reflections seen in those seismograms show the CO_2 accumulations below the mudstone layers as the injection proceeds. In particular, the pushdown effect observed in the real seismograms (Chadwick et al., 2009) due to CO_2 accumulations is clearly observed. But the seismograms obtained from the two capillary pressure curves are quite different. The difference in P-wave phase velocities and attenuation coefficients is clearly observed in Figure 4. Therefore, the influence of capillary forces is very important in CO_2 storage and a precise estimation of this curve is needed to perfom realistic long term predictions.

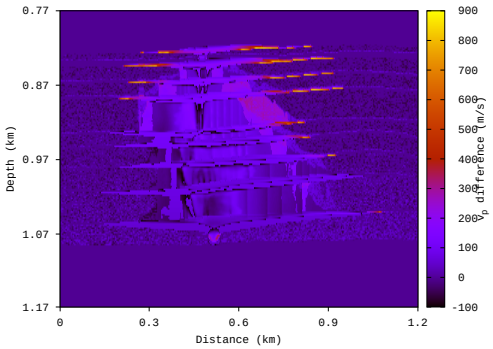

(a)

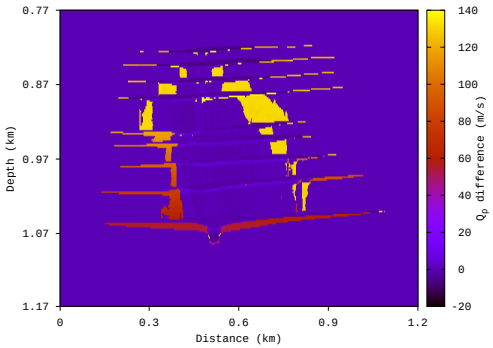

(b)

Figure 4: Difference between P-wave phase velocities and attenuation coefficients obtained with higher and lower capillary pressure

CONCLUSIONS

The fluid-flow simulator yields CO_2 accumulations below the mudstone layers and the corresponding synthetic seismograms resemble the real seismic data, where the pushdown effect is clearly observed. Capillary forces affect the migration and dispersal of the CO_2 plume; higher values of this curve cause a slower CO_2 upward migration and thicker zones of CO_2 accumulations. The influence of capillary forces is clearly observed in the synthetic seismograms.

REFERENCES

Arts, R., A. Chadwick, O. Eiken, S. Thibeau, and S. Nooner, 2008, Ten years of experience of monitoring CO_2 injection in the utsira sand at sleipner, offshore norway: First break, **26**, 65–72.

Aziz, K. and A. Settari, 1985, Petroleum reservoir simulation: Elsevier Applied Science Publishers.

Carcione, J., S. Picotti, D. Gei, G. Rossi, and J. Santos, 2012, Seismic modeling to monitor CO_2 geological storage - 1 the Atzbach-Schwanenstadt gas field: Journal of Geophysical Research, **117**, 1–18.

Carcione, J. M., 2007, Wave fields in real media: Wave propagation in anisotropic, anelastic, porous and electromagnetic media, volume **38** *of* Handbook of Geophysical Exploration: Elsevier, 2nd edition, revised and extended.

Carcione, J. M. and S. Picotti, 2006, P-wave seismic attenuation by slow-wave diffusion:Effects of inhomogeneous rock properties: Geophysics, **71**, O1–O8.

Carcione, J. M., J. E. Santos, C. L. Ravazzoli, and H. B. Helle, 2003, Wave simulation in partially frozen porous media with fractal freezing conditions: J. Appl. Physics, **94**, 7839–7847.

Chadwick, A., R. Arts, and O. Eiken, 2005, 4d seismic quantification of a growing CO_2 plume at sleipner, north sea: Dore A G and Vincent B (Eds) Petroleum Geology: North West Europe and Global Perspectives - Proc. 6th Petroleum Geology Conference, 1385–1399.

Chadwick, R., D. Noy, R. Arts, and O. Eiken, 2009, Latest time-lapse seismic data from Sleipner yield new insights into CO_2 plume development: Energy Procedia, 2103–2110.

Fanchi, J., 1997, Principles of applied reservoir simulation: Gulf Professional Publishing Company.

Frankel, A. and R. W. Clayton, 1986, Finite difference simulation of seismic wave scattering: implications for the propagation of short period seismic waves in the crust and models of crustal heterogeneity: Journal of Geophysical Research, **91**, 6465–6489.

Ha, T., J. Santos, and D. Sheen, 2002, Nonconforming finite element methods for the simulation of waves in viscoelastic solids: Comput. Meth. Appl. Mech. Engrg., **191**, 5647–5670.

Hassanzadeh, H., M. Pooladi-Darvish, A. Elsharkawy, D. Keith, and Y. Leonenko, 2008, Predicting PVT data for CO_2-brine mixtures for black-oil simulation of CO_2 geological storage: International Journal of Greenhouse Gas Control, **2**, 65–77.

Krief, M., J. Garat, J. Stellingwerff, and J. Ventre, 1990, A petrophysical interpretation using the velocities of P and S waves (full waveform sonic): The Log Analyst, **31**, 355–369.

Peng, D. and K. Robinson, 1976, A new two-constant equation of state: Ind. Eng. Chem. Fundam., **15**, 59–64.

Santos, J. E., J. G. Rubino, and C. L. Ravazzoli, 2008, Modeling mesoscopic attenuation in a highly heterogeneous biot's medium employing an equivalent viscoelastic model: Proc. 78th Annual International Meeting SEG (Las Vegas), 2212–2215.

Savioli, G. and M. S. Bidner, 2005, Simulation of the oil and gas flow toward a well - a stability analysis: Journal of Petroleum Science and Engineering, **48**, 53–69.

White, J. E., N. G. Mikhaylova, and F. M. Lyakhovitskiy, 1975, Low-frequency seismic waves in fluid-saturated layered rocks: Izvestija Academy of Siences USSR, Physics of Solid Earth, **10**, 654–659.